

Supporting Information for

New iron(II) spin-crossover metallomesogen with long aliphatic chain terminated by a C=C bond

Shuting Liu,^{a,b} Zhenhua Zhu,^a Xiao-Lei Li^a and Jinkui Tang^{*a,b}

^aState Key Laboratory of Rare Earth Resource Utilization, Changchun Institute of Applied Chemistry, Chinese Academy of Sciences, Changchun 130022, P. R. China

^bSchool of Applied Chemistry and Engineering, University of Science and Technology of China, Hefei 230026, P. R. China

Correspondence

to:

tang@ciac.ac.cn

Table of contents

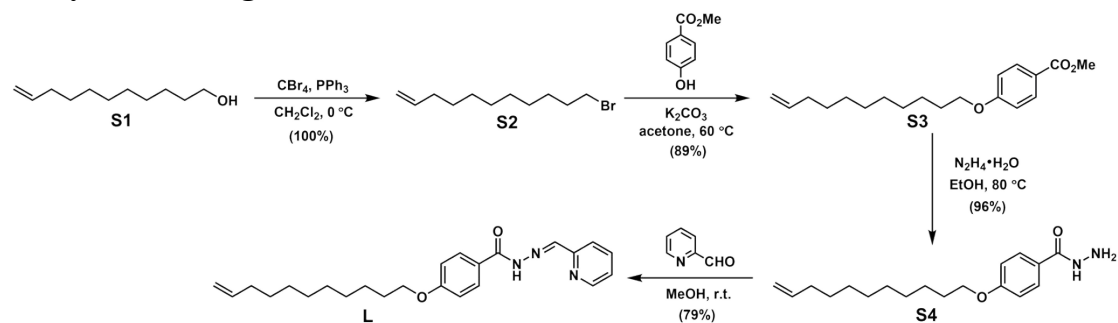
I. General procedures	2
II. Synthesis of ligand.....	4
III. Synthesis of Fe-C₁₁.....	6
IV. Characterization data for Fe-C₁₁	7
V. ¹H NMR Spectra.....	19
VI. References.....	23

I. General procedures

All reactions were carried out under dry nitrogen atmosphere with dry solvents unless otherwise stated. Dry dichloromethane (CH_2Cl_2) was refluxed and distilled over calcium hydride. Acetone was dried over Na_2CO_3 before use. Dry methanol (MeOH), ethanol (EtOH) and other reagents were purchased from commercial source and used without further purification, unless otherwise stated. Yields refer to chromatographically and spectroscopically ($^1\text{H-NMR}$) homogeneous material, unless otherwise stated. Reactions were monitored by thin layer chromatography (TLC) carried out on Shanghai Shengya Chemicals (China) plates (GF254), using UV light as the visualizing agent and/or basic potassium permanganate (KMnO_4) and heat as a developing agent. Purification by flash column chromatography was performed using Tsingdao Haiyang silica gel (200-300 mesh). **Proton nuclear magnetic resonance** ($^1\text{H-NMR}$) spectra were recorded on Bruker AV400 MHz instrument and calibrated using TMS or residual undeuterated solvent as an internal reference (0.00 ppm for TMS and 7.26 ppm for CDCl_3). The following abbreviations were used to explain the multiplicities: s = singlet, d = doublet, t = triplet, q = quartet, br = broad, m = multiplet. **Elemental analyses** (C, H, and N) were performed by PerkinElmer 2400 analyzer. **Fourier Transform infrared spectrum** (FT-IR) was recorded on a Nicolet 6700 Flex FTIR spectrometer equipped with a smart iTR attenuated total reflectance (ATR) sampling accessory and labeled according to their relative intensities with vs (very strong), s (strong), m (medium), and w (weak). **Powder X-ray diffraction** (PXRD) data were collected on a Bruker D8 advance X-ray diffractometer using $\text{Cu K}\alpha$ radiation ($\lambda = 1.54184 \text{ \AA}$) over the range of $1\text{-}50^\circ$. The variable-temperature PXRD patterns were recorded on the same instrument with a high temperature sampling accessory at $5\text{-}50^\circ$. The sample was filled in unsealed, thin-walled alumina sheet with an outer diameter of 1.3 mm and was measured from 303-463 K. **Differential scanning calorimetry** (DSC) analyses were performed on a Q20 DSC (TA Instruments) and on a DSC 3/700 (Mettler Toledo Instruments, Switzerland) over the range 300-380 K and 300-490 K, respectively. The samples were heated and cooled down at a rate of 5 K/min under an argon atmosphere. **Thermogravimetric analyses** (TGA) were performed on a Netzsch STA 449F3 analyzer under N_2 atmosphere from room temperature to 800°C at a heating rate of $10^\circ\text{C}/\text{min}$. **Polarized optical microscopy** (POM) textures were obtained using Nikon polarization microscope ECLIPSE LV100N POL with a heating/cooling rate of $10^\circ\text{C}/\text{min}$. **Mössbauer spectra** were recorded with a ^{57}Co source in a Rh matrix using an alternating constant acceleration *Wissel* Mössbauer spectrometer operated in the transmission mode and equipped with a *Janis* closed-cycle helium cryostat. Isomer shifts are given relative to iron metal at ambient temperature. Simulation of the experimental data was performed with the *Mfit* program using *Lorentzian* line doublets (E. Bill, Max-Planck Institute for Chemical Energy Conversion, Mülheim/Ruhr, Germany). **Single-crystal X-ray diffraction** (SCXRD) measurements were collected on a Bruker D8 Venture CCD diffractometer with graphite-monochromated $\text{Mo K}\alpha$ radiation ($\lambda = 0.71073 \text{ \AA}$). The crystal was successively collected at 298, 350 and 373 K, using slow heating rates (120 K/h). The program APEX3 was used to integrate the data, which were thereafter corrected for

absorption using multi-scan method. The structures were solved by intrinsic phasing methods and refined by full-matrix least-squares methods on F^2 with anisotropic thermal parameters for all non-hydrogen atoms by using the SHELXT¹ (intrinsic phasing methods) and refined by SHELXL² (full matrix least-squares techniques) in the Olex2³ package. All non-hydrogen atoms were refined with anisotropic displacement parameters. The hydrogen atoms were introduced in calculated positions and refined with a fixed geometry with respect to their carrier atoms. Crystallographic data, refinement details and CCDC number are given in Table S1. **Magnetic susceptibility measurements** were performed over the range 2-380 K using a Quantum Design MPMS-XL7 SQUID magnetometer, with an applied field of 1000 Oe in the sweep mode. For detecting the dependence of scan rate, data were recorded on the same instrument with the same field but in the temperature range 270-380 K at rates 10, 5, 2, 1 and 0.5 K/min using the sweep mode. The experimental magnetic data were corrected for the diamagnetism estimated from Pascal's constants and sample holder calibration.

II. Synthesis of ligand



Scheme S1. Synthesis of ligand

11-bromoundec-1-ene (S2): To an ice-cold solution of alcohol **S1** (7 mL, 35 mmol) and PPh₃ (10.1 g, 38.5 mmol) in CH₂Cl₂ (100 mL) was added CBr₄ (11.6 g, 35 mmol) portionwise. The resulting mixture was stirred at the same temperature for 1 h and concentrated to near dryness via rotary evaporation. The residue was purified via column chromatography (SiO₂, hexane) to give product **S2** as colorless liquid (8.15 g, 35 mmol) in 100% yield. ¹H NMR (400 MHz, CDCl₃) δ 5.89 – 5.72 (m, 1H), 5.02 – 4.90 (m, 2H), 3.40 (t, *J* = 6.9 Hz, 2H), 2.04 (q, *J* = 6.9 Hz, 2H), 1.89 – 1.80 (m, 2H), 1.47 – 1.24 (m, 12H).

Methyl-4-(undec-10-en-1-yloxy)benzoate (S3): To a solution of methyl-4-hydroxybenzoate (2.07 g, 13.6 mmol) and K₂CO₃ (1.80 g, 13.0 mmol) in acetone (25 mL) was added **S2** (1.52 g, 6.5 mmol). The mixture was heated to reflux under nitrogen atmosphere for 24 h. The mixture was filtered and the filtrate was concentrated via rotary evaporation. The residue was purified via column chromatography (SiO₂, EtOAc/hexanes = 1:20) to give product **S3** as white solid (1.75 g, 5.8 mmol) in 89% yield. ¹H NMR (400 MHz, CDCl₃) δ 7.97 (d, *J* = 8.8 Hz, 2H), 6.90 (d, *J* = 8.8 Hz, 2H), 5.81 (ddt, *J* = 16.9, 10.2, 6.7 Hz, 1H), 5.06 – 4.88 (m, 2H), 4.00 (t, *J* = 6.5 Hz, 2H), 3.88 (s, 3H), 2.04 (q, *J* = 7.0 Hz, 2H), 1.89 – 1.73 (m, 2H), 1.47 – 1.24 (m, 12H).

4-(undec-10-en-1-yloxy)benzohydrazide (S4): To a solution of **S3** (1.37 g, 4.5 mmol) in EtOH (10 mL) was added Hydrazine monohydrate (2.2 mL, 45 mmol). The mixture was heated to reflux under nitrogen atmosphere for 20 h. The resulting solution was cooled to -20 °C in fridge overnight. The solid was collected by filtration, washed with water and cold EtOH, dried under vacuum to give product **S4** as white solid (1.35 g, 4.4 mmol) in 96% yield. ¹H NMR (400 MHz, DMSO) δ 9.59 (s, 1H), 7.79 (d, *J* = 8.8 Hz, 2H), 6.96 (d, *J* = 8.8 Hz, 2H), 5.80 (ddt, *J* = 16.9, 10.2, 6.7 Hz, 1H), 4.97 (ddd, *J* = 13.7, 11.2, 1.4 Hz, 2H), 4.42 (s, 2H), 4.00 (t, *J* = 6.5 Hz, 2H), 2.01 (q, *J* = 6.9 Hz, 2H), 1.79 – 1.63 (m, 2H), 1.48 – 1.18 (m, 12H).

N'-(pyridin-2-ylmethylene)-4-(undec-10-en-1-yloxy)benzohydrazide (L): To a solution of **S4** (1.35 g, 4.4 mmol) in MeOH (20 mL) was added picolinaldehyde (0.46 mL, 4.9 mmol) at room temperature and the mixture was stirred overnight. The solid was collected by filtration, washed with cold MeOH and ether, dried under vacuum to

give product **L** as white solid (1.38 g, 3.5 mmol) in 79% yield. ¹H NMR (400 MHz, DMSO) δ 11.90 (s, 1H), 8.61 (d, *J* = 4.8 Hz, 1H), 8.47 (s, 1H), 7.98 – 7.84 (m, 4H), 7.45 – 7.37 (m, 1H), 7.06 (d, *J* = 8.7 Hz, 2H), 5.87 – 5.72 (m, 1H), 4.96 (dd, *J* = 23.6, 14.0 Hz, 2H), 4.05 (t, *J* = 6.5 Hz, 2H), 2.01 (q, *J* = 6.8 Hz, 2H), 1.72 (q, *J* = 6.9 Hz, 2H), 1.52 – 1.12 (m, 12H).

III. Synthesis of Fe-C₁₁

FeL₂ (Fe-C₁₁): Ligand L (0.1968 g, 0.5 mmol) was taken up in MeOH (15 mL) and heated to 60 °C. Triethylamine (140 μ L, 1.0 mmol) was then added and stirred at the same temperature for 15 minutes. To the pale yellow solution was then added Fe(ClO₄)₂ • xH₂O (0.0638g, 0.25 mmol), which rendered the solution dark green (**Caution!** Perchlorate salts are potentially explosive and must be handled with care and in small quantities). After 20 additional hours stirring at 60 °C, the reaction mixture was removed from the heat source and cooled to room temperature. The solid was collected by filtration, washed with small fraction of MeOH, dried under vacuum to give product **Fe-C₁₁** as black solid (133 mg, 0.158 mmol) in 63% yield. The rod-shaped black crystals suitable for single crystal diffraction were obtained by slow cooling hot reaction solution. Elemental analyses - Calc. (Found) for C₄₈H₆₀FeN₆O₄: C, 68.56 (68.64); N, 9.99 (9.69), H, 7.19 (7.44). Selected FT-IR data (ATR, cm⁻¹): 3060 (m), 2917 (s), 2849 (s), 2612 (w), 2554 (w), 2422 (w), 1642 (m), 1602 (s), 1583 (w), 1562 (w), 1520 (s), 1470 (s), 1443 (s), 1404 (m), 1357 (vs), 1293 (m), 1246 (vs), 1208 (w), 1166 (vs), 1145 (w), 1108 (s), 1063 (s), 1037 (w), 1020 (w), 1012 (m), 991 (m), 920 (m), 907 (m), 851 (w), 841 (m), 818 (m), 759 (s), 724 (m), 698 (w), 685 (s), 656 (w), 644 (w), 633 (w), 576 (m), 546 (m), 533 (w).

IV. Characterization data for Fe-C₁₁

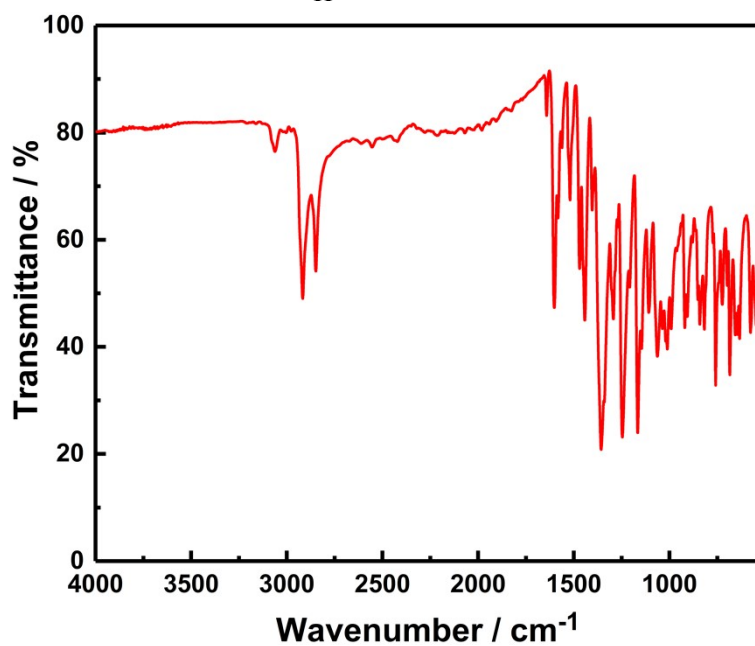


Figure S1. FT-IR spectrum of a solid sample of Fe-C₁₁.

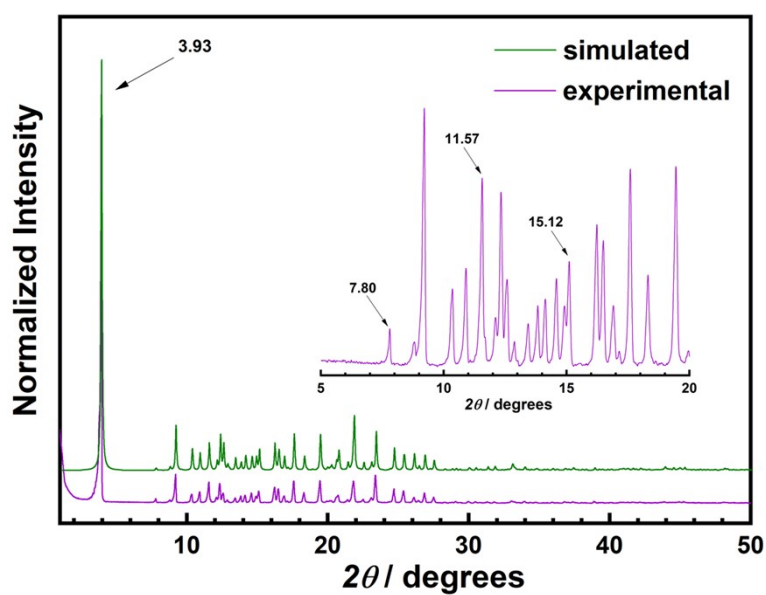


Figure S2. Experimental (purple) and simulated (green) PXRD patterns for Fe-C₁₁ in the range of 1-50° (inset: experimental pattern in the range of 5-20°). The arrows indicate four reflections at $2\theta = 3.93, 7.80, 11.57$ and 15.12° , respectively.

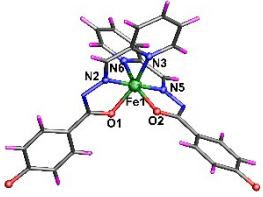
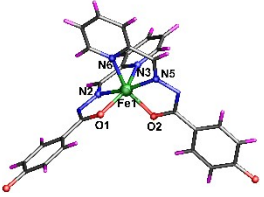
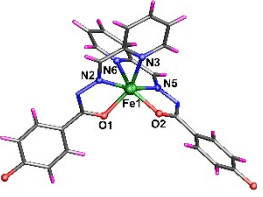
Table S1. Crystallographic data of complex Fe-C₁₁ at 298, 350 and 373 K

Temperature, K	298	350	373
empirical formula		C ₄₈ H ₆₀ FeN ₆ O ₄	
formula weight, g·mol ⁻¹		840.87	
crystal size, mm ³		0.08 x 0.20 x 0.28	
crystal system		Triclinic	
space group		<i>P</i> $\bar{1}$	
λ , Å		0.71073	
<i>a</i> , Å	9.2662(4)	9.1950(4)	8.921(2)
<i>b</i> , Å	10.9952(4)	11.1984(5)	11.118(3)
<i>c</i> , Å	22.8338(9)	23.1034(11)	24.709(6)
α , °	86.6740(10)	87.452(2)	81.936(7)
β , °	89.749(2)	87.594(2)	83.521(7)
γ , °	85.972(2)	84.078(2)	82.046(7)
<i>V</i> , Å ³	2316.74(16)	2362.23(19)	2392.2(10)
<i>Z</i>	2	2	2
ρ (cal), g·cm ⁻³	1.205	1.182	1.167
$\mu_{MoK\alpha}$, mm ⁻¹	0.374	0.366	0.362
<i>F</i> (000)	896	896	896
2 θ range [°]	4.032 to 52.05	3.998 to 52.164	3.888 to 52.094
<i>T</i> min / <i>T</i> max	0.914/0.971	0.916/0.971	0.917/0.971
measured refl.	26722	26931	39253
unique refl. [<i>R</i> int]	9081, 0.0430	9253, 0.0534	9301, 0.1162
data/restraints/parameters	9081/9/532	9253/29/532	9301/206/532
<i>R</i> 1, <i>wR</i> 2 (<i>I</i> > 2 σ (<i>I</i>)) ^{a,b}	0.0552, 0.1428	0.0690, 0.1749	0.0832, 0.2151
<i>R</i> 1, <i>wR</i> 2 (all data)	0.0816, 0.1637	0.1217, 0.2020	0.1660, 0.2704
goodness-of-fit (<i>F</i> ²) ^c	1.044	1.016	1.029
res. el. dens. [e·Å ⁻³]	0.478 / -0.444	0.343 / -0.390	0.421 / -0.497
CCDC number	2105602	2105603	2105604

^a $I > 2\sigma(I)$, $R_1 = \sum(|F_o| - |F_c|)/\sum|F_o|$. ^b $wR_2 = \{\sum[w(F_o^2 - F_c^2)^2]/\sum[w(F_o^2)^2]\}^{1/2}$.

^c (goodness of fit on *F*²) = $\{\sum[w(F_o^2 - F_c^2)^2]/(n-p)\}^{1/2}$, where *n* is the number of reflections and *p* is the total number of refined parameters.

Table S2. Coordination sphere parameters for Fe-C₁₁ at 298, 350 and 373 K

	Triclinic $P\bar{1}$ (298 K)		Triclinic $P\bar{1}$ (350 K)		Triclinic $P\bar{1}$ (373 K)	
						
Fe-N _{py} / Å	Fe1-N3	1.962(2)	Fe1-N3	2.181(3)	Fe1-N3	2.199(4)
	Fe1-N6	1.983(2)	Fe1-N6	2.124(3)	Fe1-N6	2.265(4)
Fe-N _{imine} / Å	Fe1-N5	1.873(2)	Fe1-N5	2.037(3)	Fe1-N5	2.113(4)
	Fe1-N2	1.874(2)	Fe1-N2	2.040(3)	Fe1-N2	2.111(4)
Fe-O / Å	Fe1-O1	1.9764(18)	Fe1-O1	2.069(3)	Fe1-O1	2.062(4)
	Fe1-O2	2.010(2)	Fe1-O2	2.036(3)	Fe1-O2	2.097(3)
Bond angles / °	O1-Fe1-O2	90.93(8)	O1-Fe1-N6	93.03(11)	O1-Fe1-O2	96.24(14)
	O1-Fe1-N6	92.62(8)	O1-Fe1-N3	150.45(11)	O1-Fe1-N2	73.49(14)
	N3-Fe1-O1	159.97(9)	O2-Fe1-O1	96.19(10)	O1-Fe1-N5	110.49(14)
	N3-Fe1-O2	90.41(9)	O2-Fe1-N6	150.68(12)	O1-Fe1-N6	96.14(14)
	N3-Fe1-N6	93.07(9)	O2-Fe1-N3	95.08(11)	O1-Fe1-N3	146.97(14)
	N6-Fe1-O2	159.58(9)	O2-Fe1-N2	108.42(11)	O2-Fe1-N2	123.95(14)
	N5-Fe1-O1	99.95(8)	O2-Fe1-N5	74.88(11)	O2-Fe1-N5	73.39(14)
	N5-Fe1-O2	79.11(9)	N6-Fe1-N3	90.33(11)	O2-Fe1-N6	146.65(13)
	N5-Fe1-N3	99.93(9)	N2-Fe1-O1	75.12(11)	O2-Fe1-N3	97.27(14)
	N5-Fe1-N6	80.47(9)	N2-Fe1-N6	100.83(11)	N2-Fe1-N5	162.32(15)
	N5-Fe1-N2	177.20(11)	N2-Fe1-N3	75.41(12)	N2-Fe1-N6	89.28(14)
	N2-Fe1-O1	79.38(8)	N5-Fe1-O1	116.30(12)	N2-Fe1-N3	73.95(15)
	N2-Fe1-O2	103.60(10)	N5-Fe1-N6	76.08(12)	N5-Fe1-N6	73.27(15)
	N2-Fe1-N3	80.89(9)	N5-Fe1-N3	93.01(12)	N5-Fe1-N3	102.22(15)
	N2-Fe1-N6	96.82(10)	N5-Fe1-N2	168.09(13)	N3-Fe1-N6	88.83(14)
Σ^a / °		87.48		131.7		154.1
Θ^b / °		300.08		384.64		489.18
V_{FeN4O2}^c / Å ³		9.51		11.12		11.74

^a The octahedral distortion parameter, Σ , is determined by $\Sigma = \sum_{i=1}^{12} |90 - \varphi_i|$, where φ_i are 12 *cis* bond angles of the iron(II) coordination sphere.⁴

^b The trigonal distortion parameter, Θ , is calculated as $\Theta = \sum_{i=1}^{24} |60 - \theta_i|$, where θ_i represents the 24 trigonal angles defined by opposite faces of the octahedron.⁵

^c V_{FeN4O2} corresponds to the volume of the octahedron formed by the six coordinated atoms.

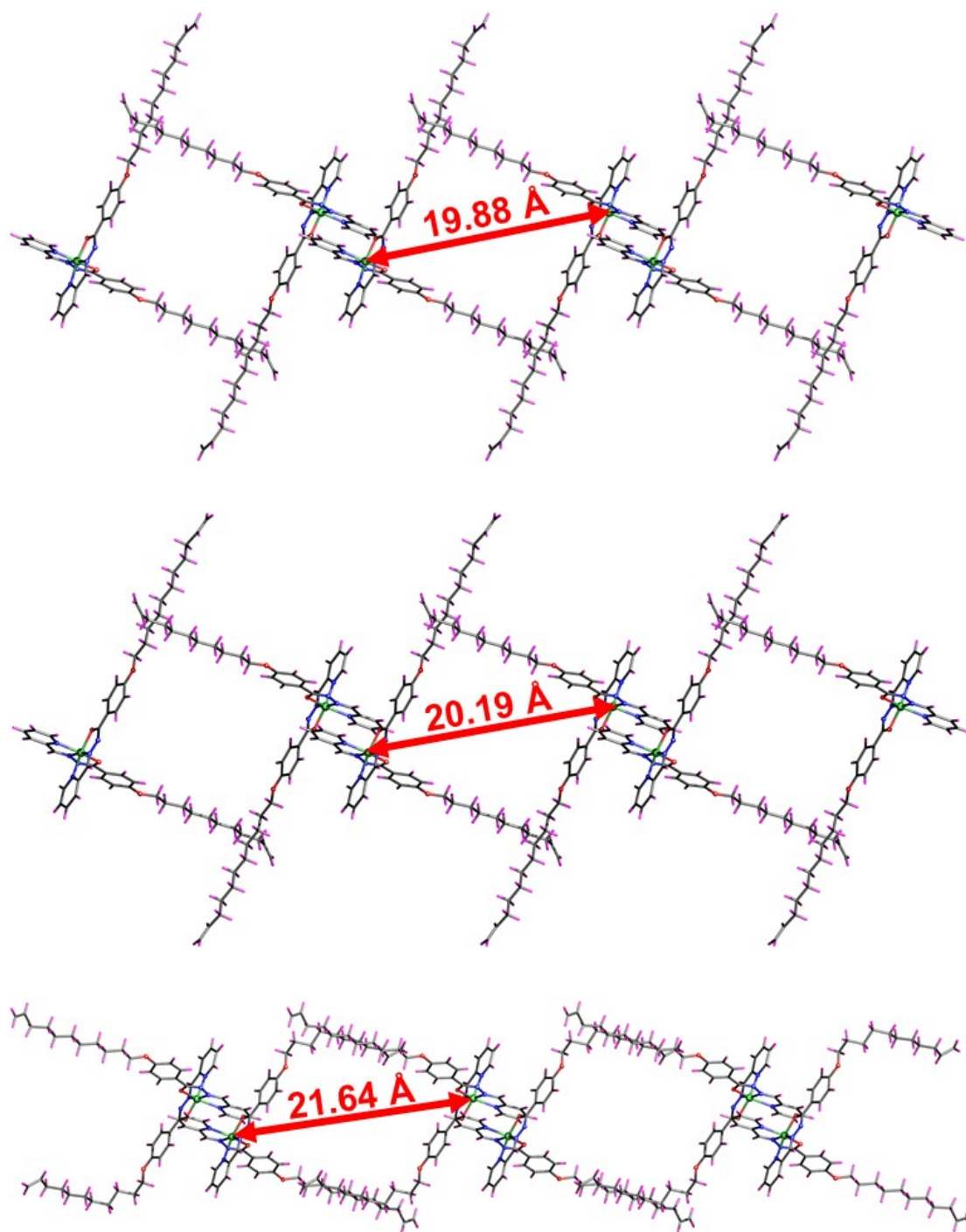


Figure S3. Projection of the packing of Fe-C₁₁ viewed along the *b*-axis at 298 (top), 350 (middle) and 373 K (bottom). Atom colors: Fe green, N blue, O red, C grey, H magenta.

Table S3. Selected intermolecular interactions and interatomic distances for Fe-C₁₁.

Temperature /K	298 K		350 K		373 K	
C-H \cdots O (C \cdots O) /Å	C21-H21 \cdots O3	2.706	C12-H12 \cdots O4	2.640	C17-H17 \cdots O3	2.576
	C18-H18 \cdots O1	2.661	C13-H13 \cdots O2	2.692	C20-H20 \cdots O1	2.620
	C23-H23B \cdots O1	2.513			C5-H5 \cdots O2	2.714
C-H \cdots N (C \cdots N) /Å	C14-H14 \cdots N4	2.500	C8-H8 \cdots N4	2.730	C10-H10 \cdots N1	2.737
	C19-H19 \cdots N1	2.503	C19-H19 \cdots N1	2.646	C19-H19 \cdots N4	2.674
C-H \cdots π (C \cdots π) /Å			C47-H47A \cdots C47	2.535		
$\pi\cdots\pi$ /Å	C3 \cdots C16	3.375	C47 \cdots C47	3.135	C1 \cdots C11	3.398
	C16 \cdots C16	3.319				
H \cdots H /Å	H23A \cdots H9	2.395	H47A \cdots H47A	2.181		
	H47B \cdots H47B	2.380	H47A \cdots H47B	2.301		
	H34B \cdots H47A	2.225				
Fe \cdots Fe _{min} /Å	Fe1 \cdots Fe1	6.679	Fe1 \cdots Fe1	6.450	Fe1 \cdots Fe1	5.896

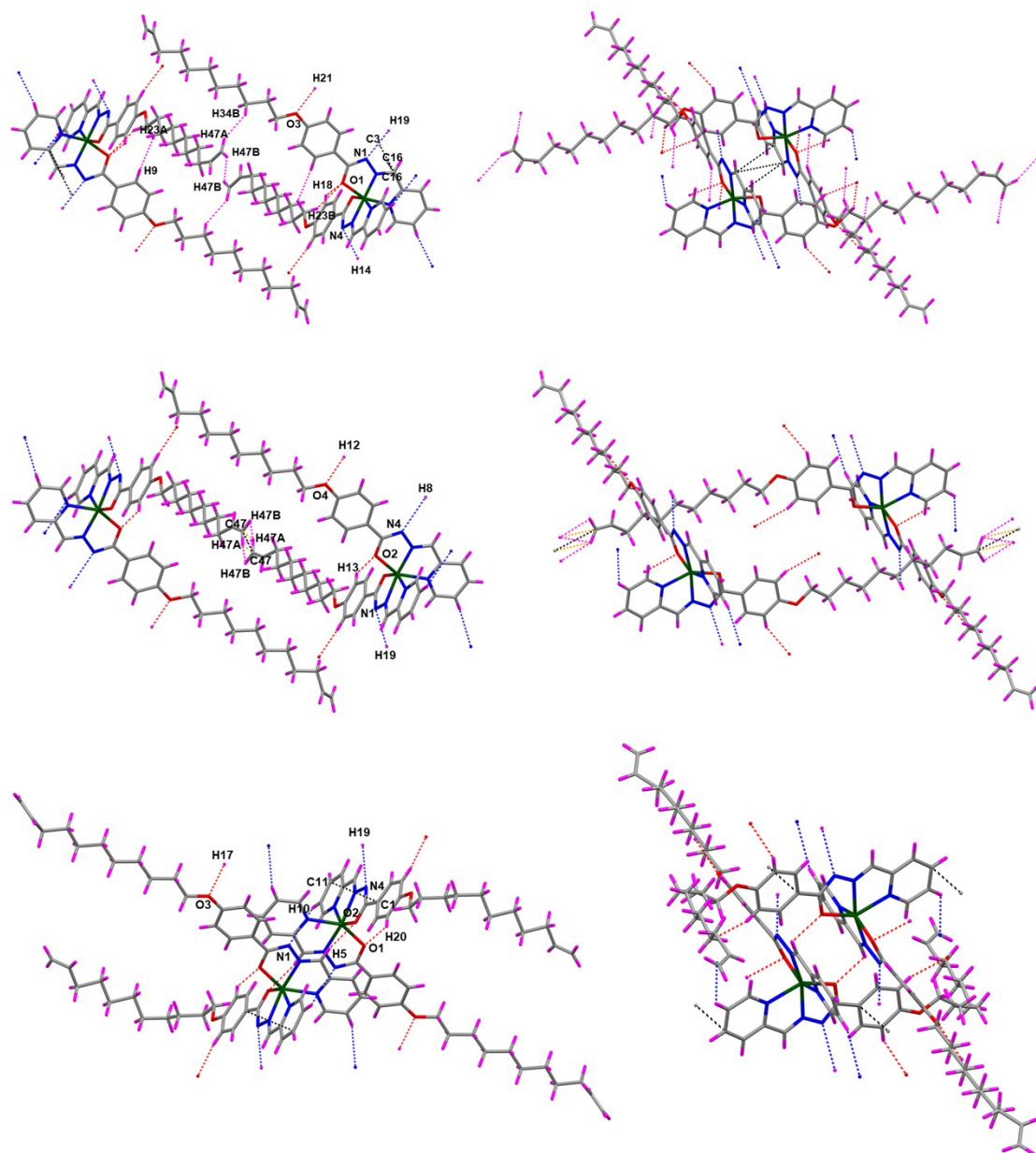


Figure S4. Intermolecular interactions (inferior to the sum of van der Waals radii) of the Fe-C₁₁, viewed along the *a* (left) and *c* (right) axes at 298 (top), 350 (middle) and 373 K (bottom). Atom colors: Fe green, N blue, O red, C grey, H magenta. Short contacts are shown as dashed lines: C-H \cdots O red, C-H \cdots N blue, C-H \cdots π orange, $\pi\cdots\pi$ black, H \cdots H magenta.

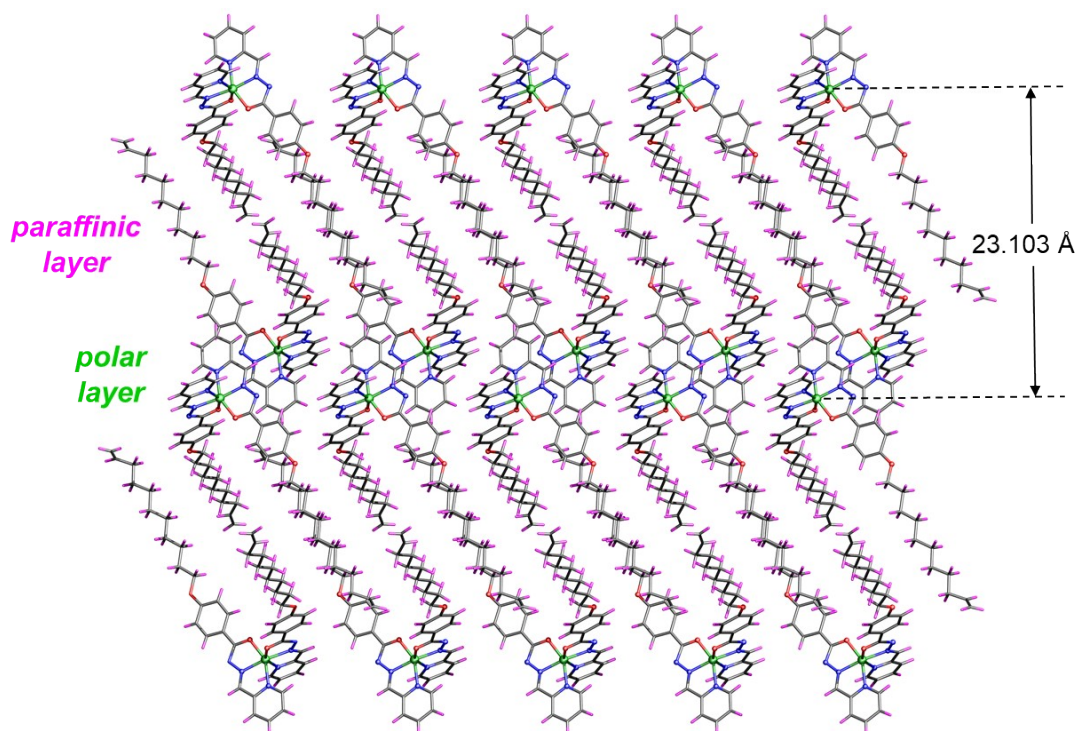


Figure S5. Projection of the molecular packing at 350 K along the *a*-axis.

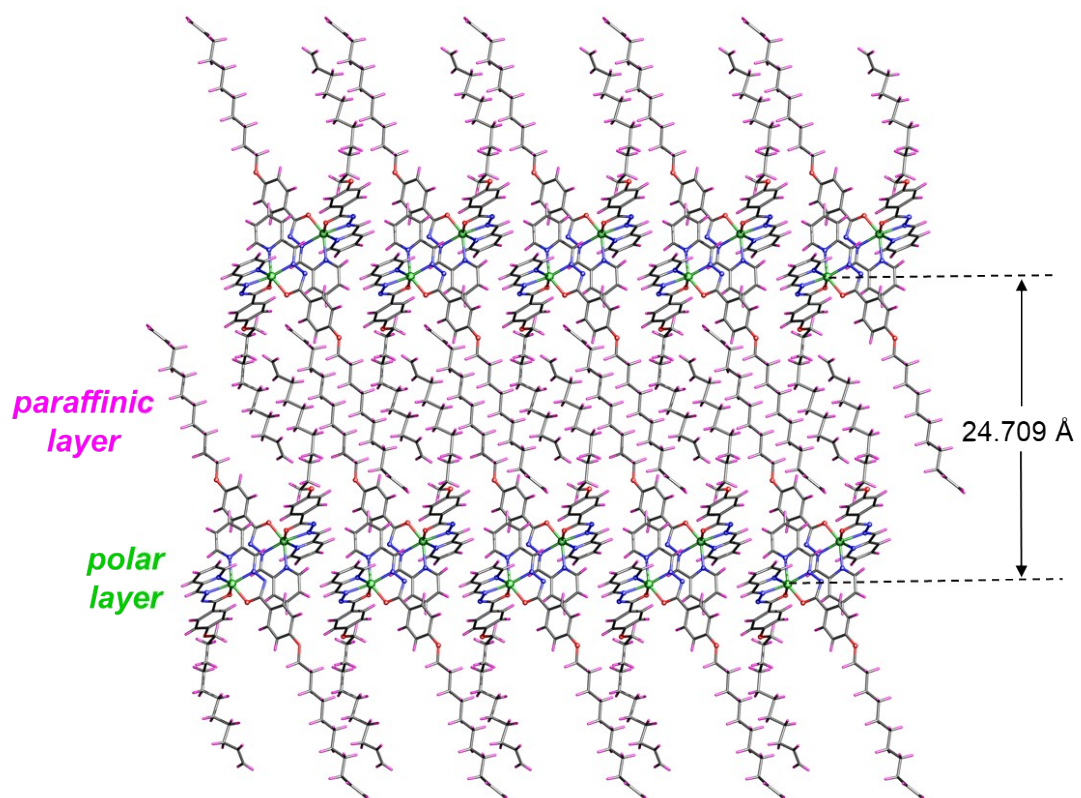


Figure S6. Projection of the molecular packing at 373 K along the *a*-axis.

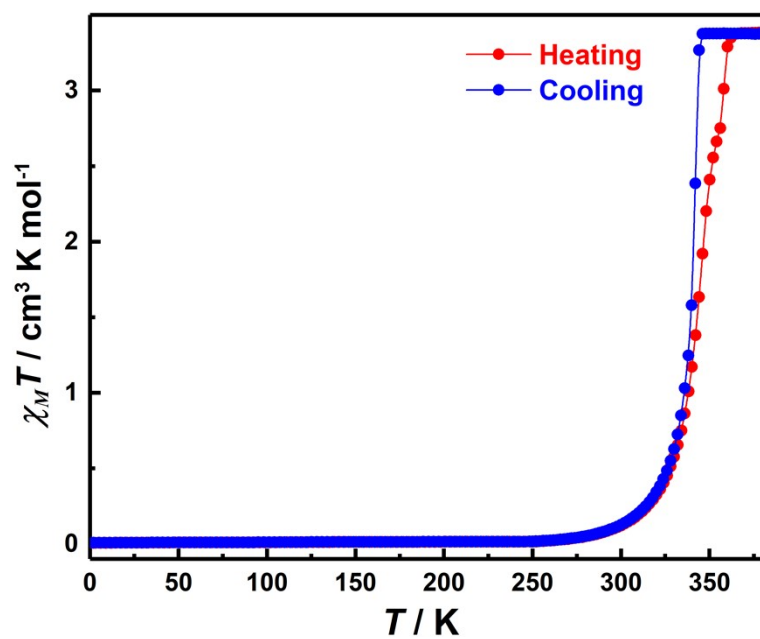


Figure S7. Temperature dependence of the $\chi_M T$ values at 1000 Oe for Fe-C₁₁ over the 2-380 K range (0.5 K/min).

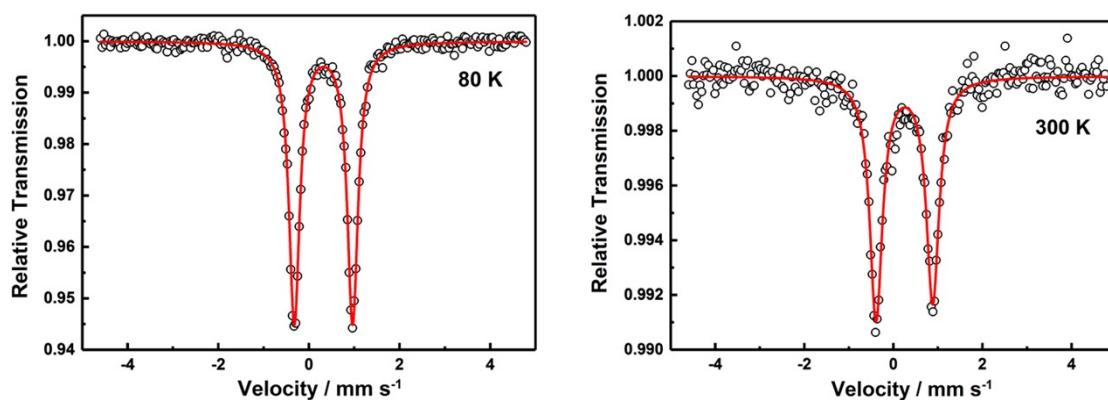


Figure S8. ^{57}Fe Mössbauer spectra for Fe-C₁₁ at 80 and 300 K. The red lines are the fit curves to the experimental data.

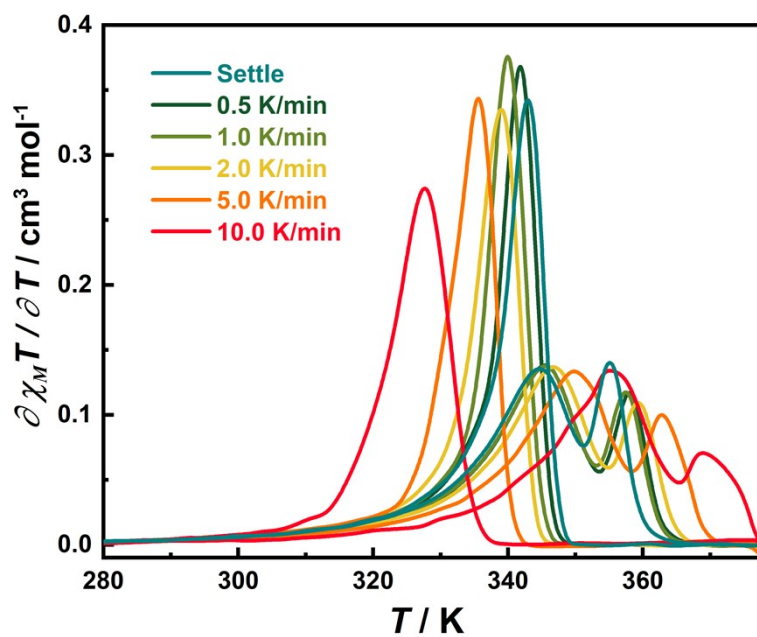


Figure S9. Temperature dependence of the $\partial\chi_M T / \partial T$ values in sweep mode (scan rate: 0.5-10 K/min) and settle mode for Fe-C₁₁.

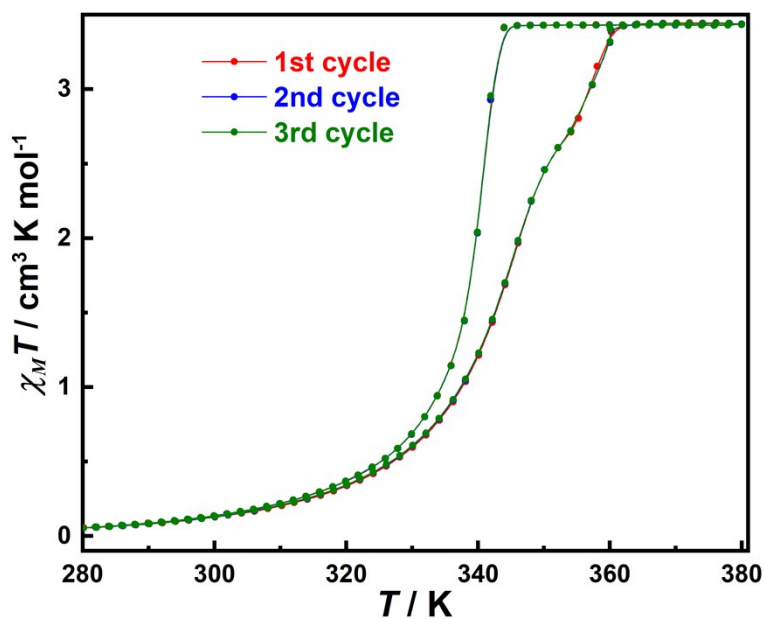


Figure S10. Temperature dependence of the $\chi_M T$ values for Fe-C₁₁, demonstrating its reversibility over the temperature range 280-380 K (scan rate: 0.5 K min⁻¹).

Table S4. DSC data and thermodynamic parameters for Fe-C₁₁.

Mode ^a	<i>T</i> / K ^b	ΔH / KJ mol ⁻¹	ΔS / J K ⁻¹ mol ⁻¹	<i>T</i> / K ^c
Heating ^{c,d}	344, 358	20.50	58.28	350, 363
Cooling	338	-20.84	-61.66	336

^a Heating/Cooling at a rate of 5 K min⁻¹.

^b Data extracted from DSC results; ^c Values estimated from magnetic measurements.

^c $\Delta H = \Delta H_1 + \Delta H_2$; ^d $\Delta S = \Delta S_1 + \Delta S_2$.

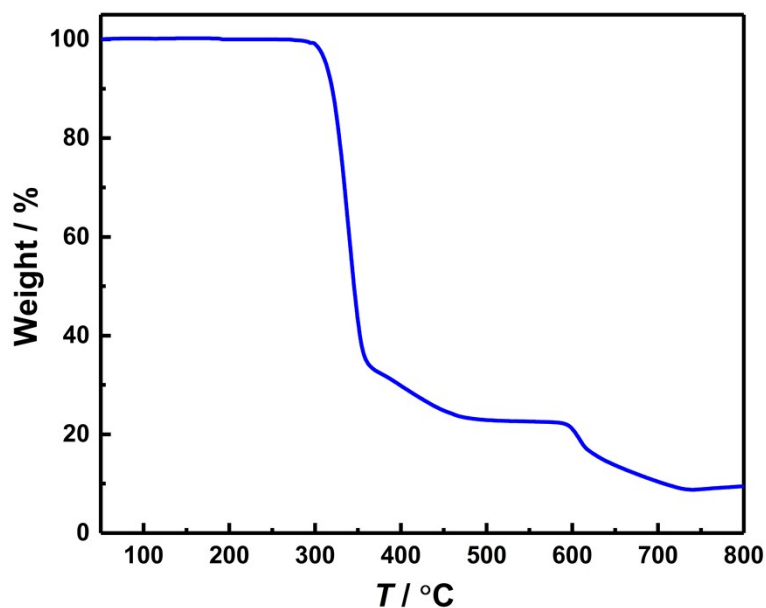


Figure S11. Thermogravimetric analysis for Fe-C₁₁.

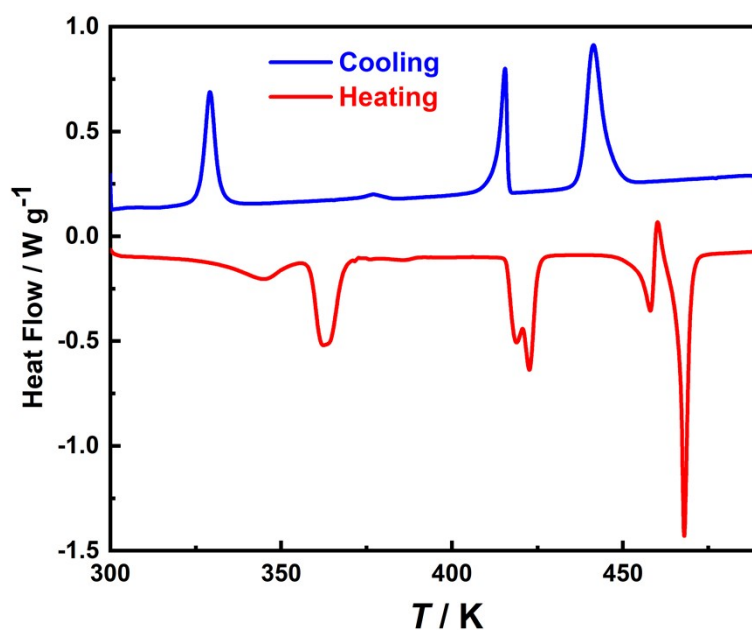


Figure S12. DSC curves for Fe-C₁₁ in the 300-490 K range at a rate of 5 Kmin⁻¹ (DSC 3/700).

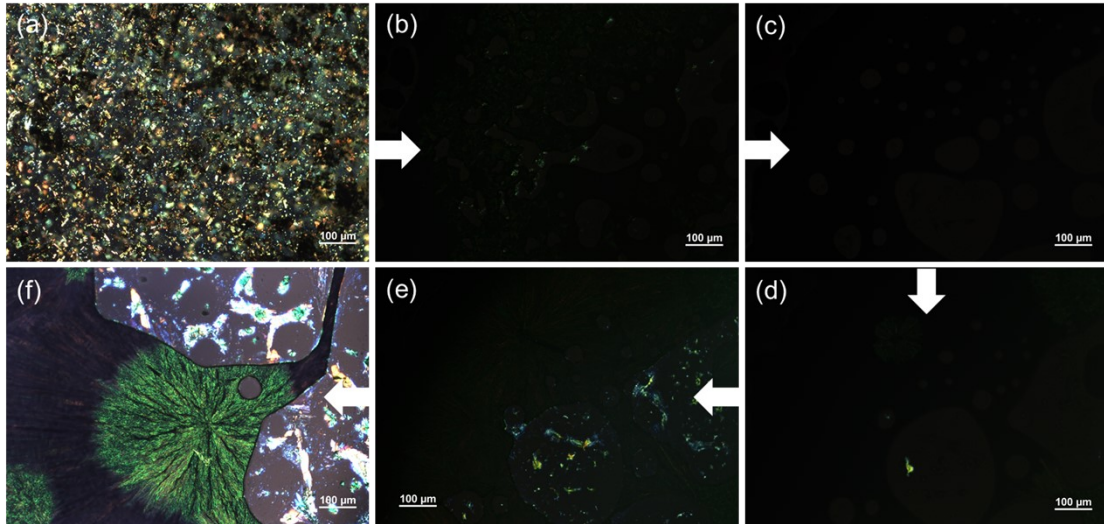


Figure S13. Optical textures of Fe-C₁₁ recorded between 298 K and 483 K on heating/cooling cycle: (a) 423 K, heating mode; (b) 463 K, heating mode; (c) 483 K, heating mode; (d) 433 K, cooling mode; (e) 363 K, cooling mode; (f) 298 K, cooling mode. The arrows are guide for the phase transition process.

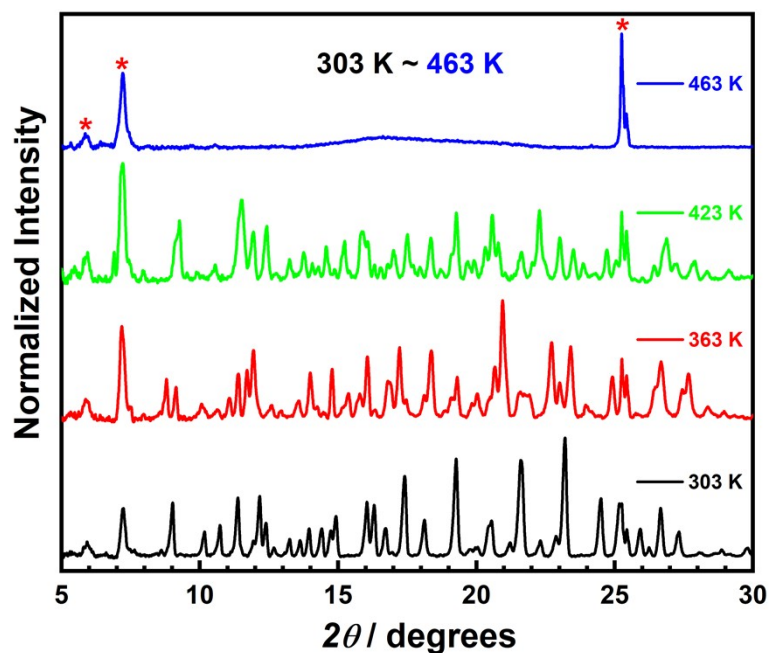


Figure S14. Variable-temperature PXRD patterns of Fe-C₁₁ measured between 303 and 463 K on heating mode (* represents the reflections of sample holder at $2\theta = 6.0, 7.2$ and 25.3°).

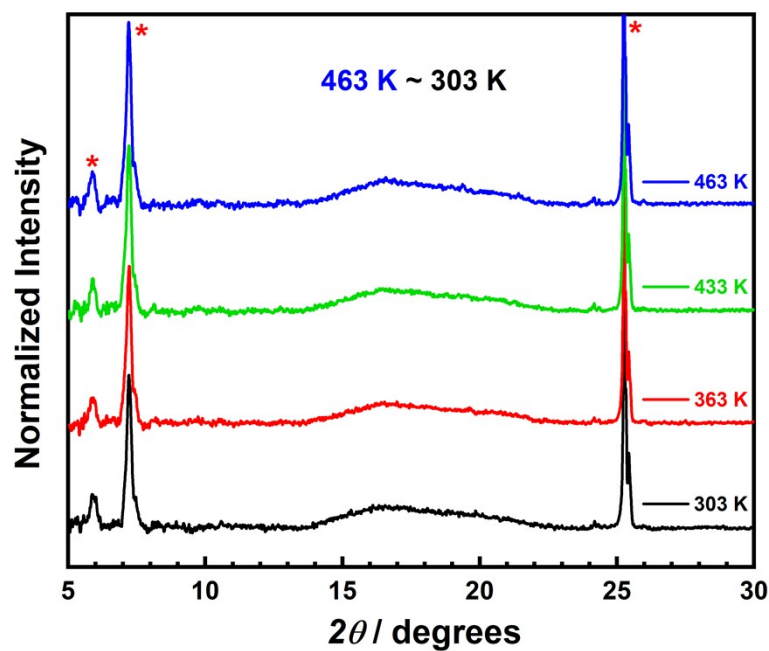
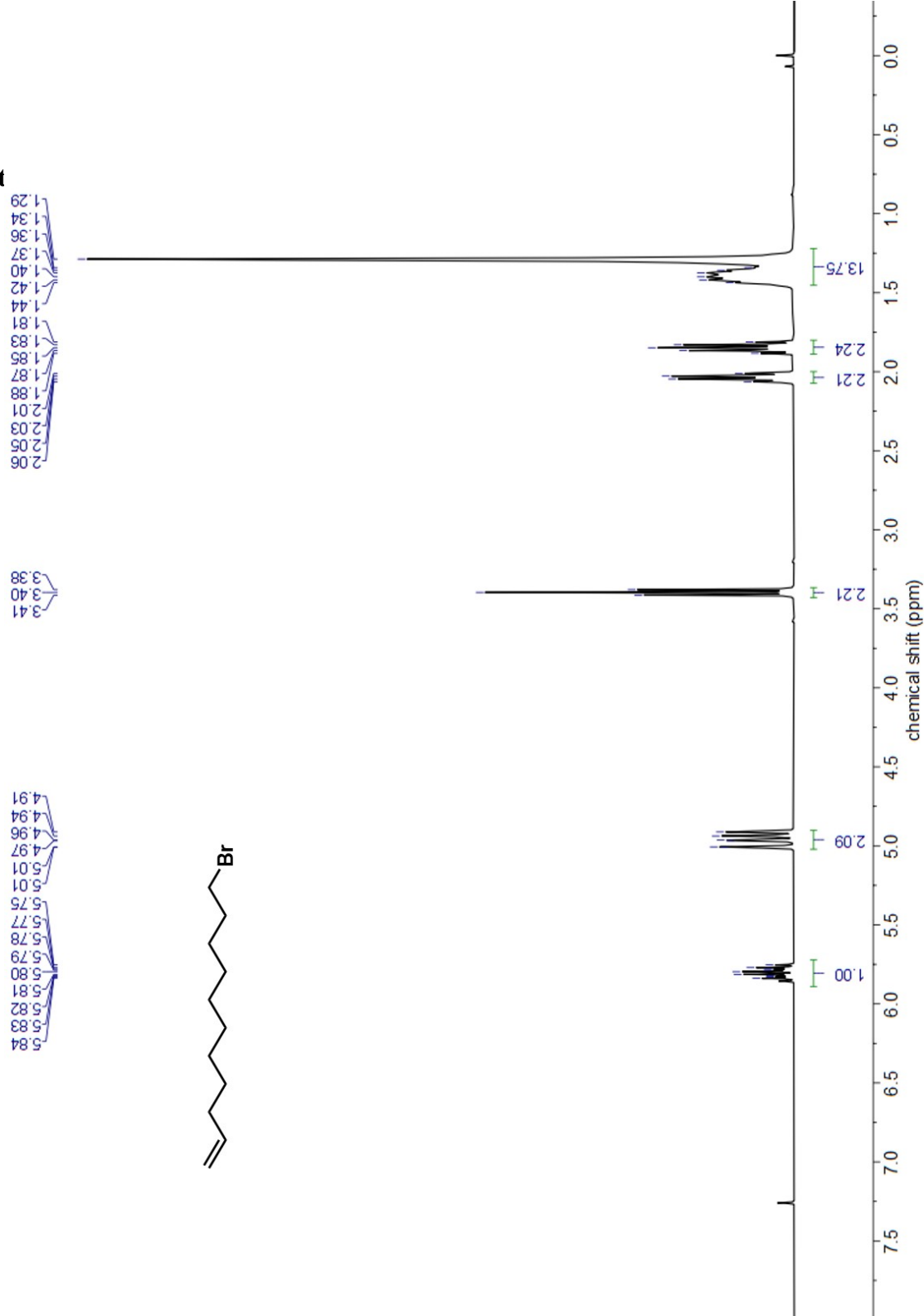
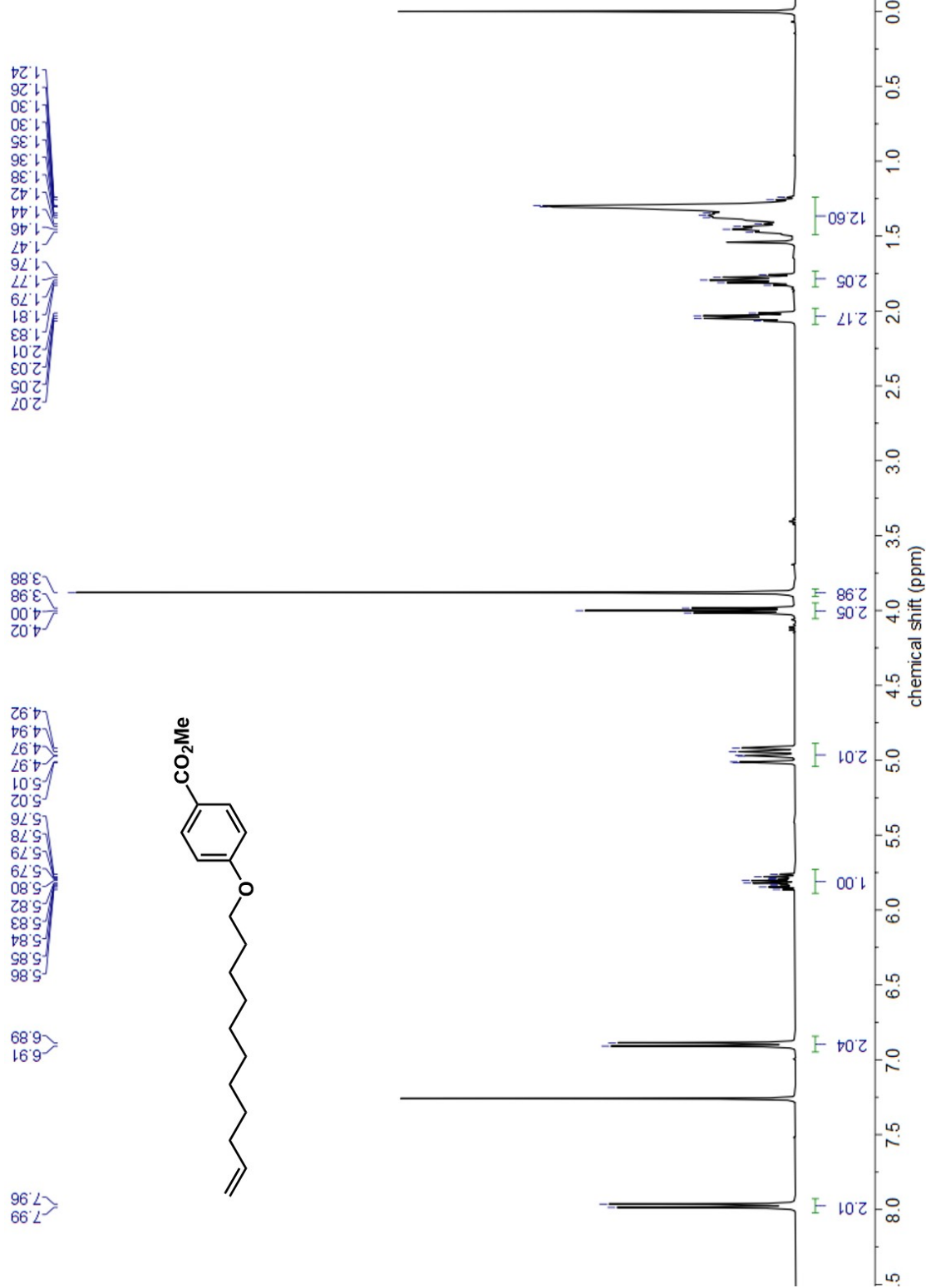
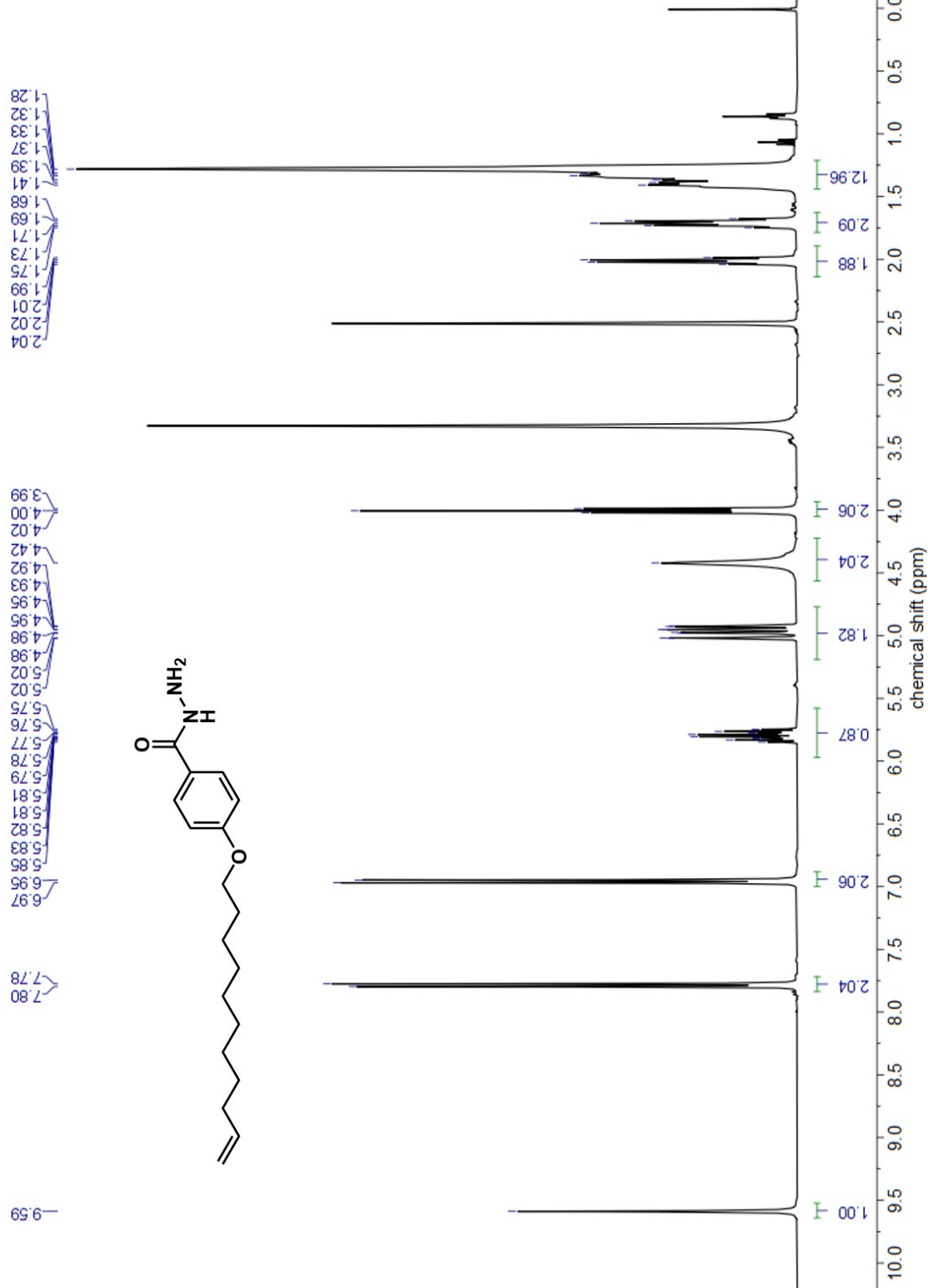


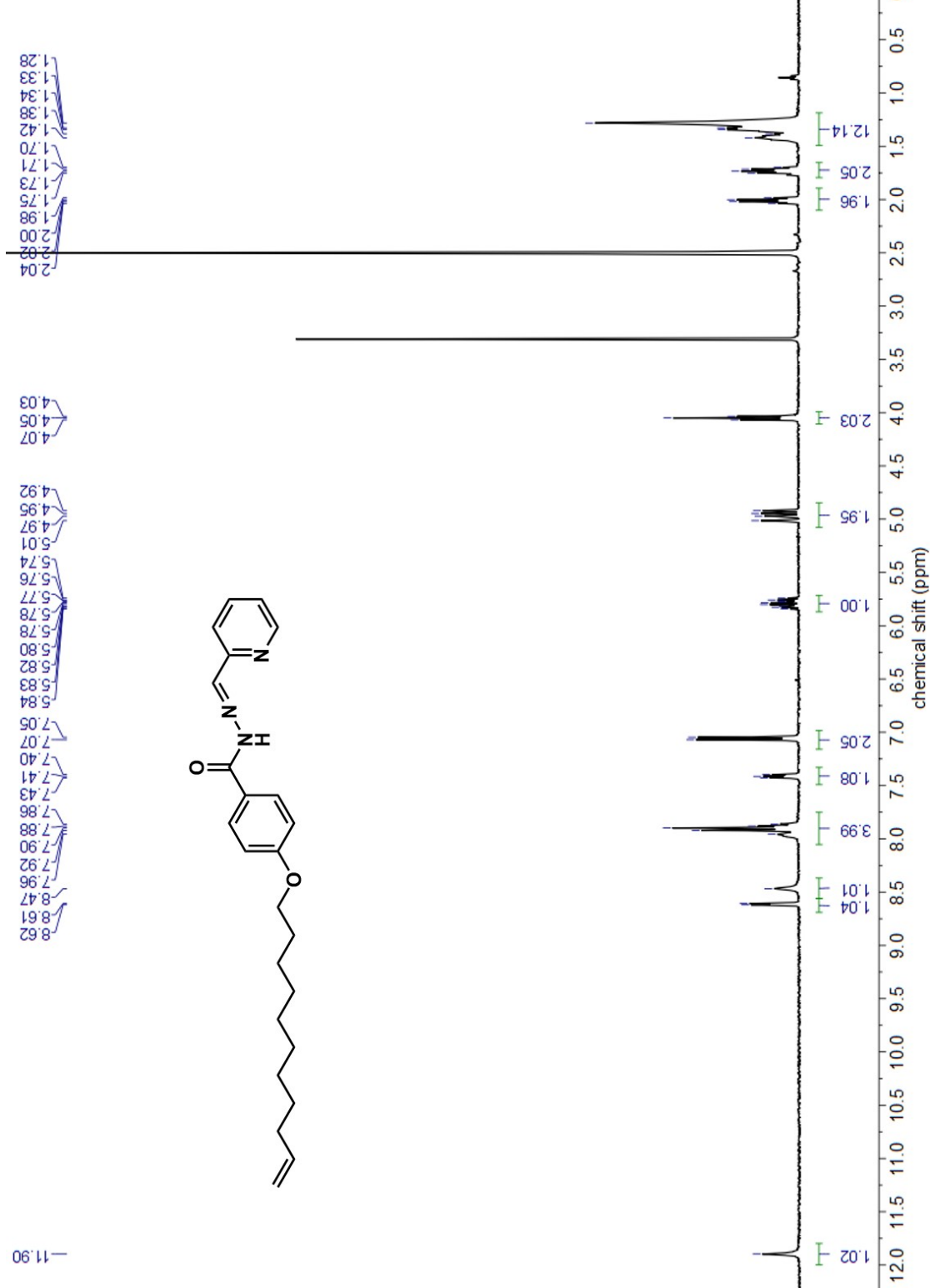
Figure S15. Variable-temperature PXRD patterns of Fe-C₁₁ measured between 463 and 303 K on cooling mode (* represents the reflections of sample holder at $2\theta = 6.0, 7.2$ and 25.3°).

V. ¹H NMR Spect









VI. References

1. G. M. Sheldrick, SHELXT - Integrated space-group and crystal-structure determination, *Acta Cryst. A*, 2015, **71**, 3-8.
2. G. M. Sheldrick, A short history of SHELX, *Acta Cryst. A*, 2008, **64**, 112-122.
3. O. V. Dolomanov, L. J. Bourhis, R. J. Gildea, J. A. K. Howard and H. Puschmann, OLEX2: a complete structure solution, refinement and analysis program, *J. Appl. Crystallogr.*, 2009, **42**, 339-341.
4. P. Guionneau, M. Marchivie, G. Bravic, J.-F. Létard and D. Chasseau, Co(II) molecular complexes as a reference for the spin crossover in Fe(II) analogues, *J. Mater. Chem.*, 2002, **12**, 2546-2551.
5. M. Marchivie, P. Guionneau, J.-F. Letard and D. Chasseau, Photo-induced spin-transition: the role of the iron(II) environment distortion, *Acta Cryst. B*, 2005, **61**, 25-28.